

Synthesis of MgO Nanoparticles from Different Organic Precursors; Catalytic Decontamination of Organic Pollutants and Antitumor Activity

Islam MI Moustafa^{1*}, Ihab A Saleh¹ and Mohamed R Abdelhamid²

¹Chemistry Department, Faculty of Science, Benha University, 13518, Egypt

²Department of Medicine and Hepatology, Faculty of Medicine, Minia University, Egypt

Abstract

The present work deals with the synthesis of nanostructured MgO from different organic precursors, by a facile precipitation method as catalysts for the decontamination of Malathion (stimulant of chemical warfare agents) (VX) and orange G as organic pollutants. The as-prepared nanoparticles were obtained by thermal decomposition of the oxalate, tartarate, citrate, succinate, malate, malonate and glycinate precursors at $\approx 650^\circ\text{C}$ and were characterized by thermal analysis, FTIR, X-ray diffraction, high resolution transmission electron microscope (HRTEM) and absorption spectra. The morphology and crystal sizes were found to be highly affected by the starting organic precursors. The results revealed that the prepared inexpensive magnesium oxides have high potential as catalysts for photo degradation of both Malathion and orange G from water samples. Inhibitory activity against Breast Carcinoma MCF-7 cell line was detected using some selected nanosized MgO and compared to that of Vinblastine as a standard drug.

Keywords: Nano sized MgO; Catalytic photo degradation; VX stimulant (Malathion); Orange G; Antitumor activity

Introduction

Researches on the synthesis and application of nanomaterials had experienced tremendous growth in recent years, owing to their unique properties making them suitable for applications in almost every field of science [1-11]. Photocatalytic degradation of dyes and toxic organic materials from aqueous solution is considered one of the most effective methods for water treatment especially using nanosized metal oxides as catalysts [12-18]. Nanocrystalline MgO is an interesting functional material due to its low heat capacity, chemical inertness, optical transparency and high thermal stability. Due to its high surface area, it is used as an efficient adsorbent for numerous toxic chemicals and acid gases. Recently, MgO nanoparticles have shown promise for application in tumor treatment and also have considerable potential as an antibacterial agent [19-24]. In the present work and in continuity to our previous work [25], we study the effect of starting organic precursors on the crystal size and morphology of nanosized MgO. The prepared nanooxides were tested successfully as adsorbents for the decontamination of Malathion as stimulant of chemical warfare agents (CWA) (VX) and orange G as organic pollutant. Inhibitory activity against Breast Carcinoma MCF-7 cell line was also tested using some selected nanosized MgO.

Experimental Section

Synthesis of magnesium oxide nanoparticles

AR grade chemicals obtained from Merck and Aldrich were used for the preparation of the nano particles of magnesium oxide (M1-M7). The individual oxides were prepared via the precipitation method by titration of 50 ml of 0.1 M magnesium acetate drop by drop to 50 ml of 0.2 M of different organic acids viz. oxalic acid (M1), tartaric acid (M2), citric acid (M3), succinic acid (M4), malic acid (M5), malonic acid (M6) and glycine (M7), respectively. The mixtures were stirred for 1 hr. and the precipitates formed were filtered, washed thoroughly using bidistilled water, air dried, thoroughly grounded in agate mortar and finally dried at 120°C for two hours in the form of fine powder. The powder so obtained was annealed at 650°C for six hours in muffle furnace to obtain the corresponding nanosized magnesium oxides.

Physical measurements

FT-IR spectra of both of the precipitated and ignited samples were recorded on a Nicolet iSio FT-IR spectrophotometer in the $4000\text{-}400\text{ cm}^{-1}$ region using KBr disk technique (Chemistry department, Faculty of science, Benha University, Egypt). Electronic absorption spectra of the prepared nanooxides were recorded on a Jasco (V-530) UV-Vis spectrophotometer (Chemistry department, Faculty of Science, Benha University, Egypt). Thermogravimetric analysis (TG-DT) for the organic precursors was recorded on Shimadzu TA-60 WS thermal analysis (Micro analytical unit, Menofia University, Shebin El-Kom, Egypt). Elemental analysis for C and H of the nanooxides were carried out using Elementer Vario EL III Carlo Erba 1108 instrument (The Regional Center for Mycology and Biotechnology, Al-Azhar University, Cairo, Egypt). X-ray powder diffraction (XRD) was recorded on a 18 kW diffractometer (Bruker; model D8 Advance) with monochromated Cu K_α radiation (λ) 1.54178 Å (Central metallurgical research institute, Helwan, Egypt). The HR-TEM images of some selected nanooxides were taken on a transmission electron microscope (JEOL; model 1200 EX) at an accelerator voltage of 220 kV (Egyptian Petroleum Research Institute, Cairo, Egypt).

Photocatalytic degradation of Orange G dye

For a typical photocatalytic experiment, 100 mg of the nanosized photocatalyst was added to 25 ml of 20 ppm aqueous dye solution which was kept in dark for 6 hrs to allow the system to reach an adsorption desorption equilibrium then 2 ml of 0.5 M hydrogen peroxide solution was added. The degradation process was investigated in a Pyrex beaker under the UV illumination using a 250 W xenon arc lamp (Thoshiba, SHLS-002) ($\lambda=365\text{ nm}$). After recovering the catalyst by centrifugation,

***Corresponding author:** Islam MI Moustafa, Chemistry Department, Faculty of Science, Benha University, 13518, Egypt, Tel/Fax: +20133222578; E-mail: islamshahin84@outlook.com

Received June 28, 2017; Accepted July 06, 2017; Published July 16, 2017

Citation: Moustafa IMI, Saleh IA, Abdelhamid MR (2017) Synthesis of MgO Nanoparticles from Different Organic Precursors; Catalytic Decontamination of Organic Pollutants and Antitumor Activity. J Material Sci Eng 6: 359. doi: [10.4172/2169-0022.1000359](https://doi.org/10.4172/2169-0022.1000359)

Copyright: © 2017 Moustafa IMI, et al. This is an open-access article distributed under the terms of the Creative Commons Attribution License, which permits unrestricted use, distribution, and reproduction in any medium, provided the original author and source are credited.

the absorption spectra of the clear solution was measured at 485 nm (λ_{\max} for Orange G dye) at different time intervals using a UV-Vis spectrophotometer.

Photocatalytic degradation of Malathion

The photocatalytic degradation of 0.06 ml/l of Malathion solution was performed using the smallest crystal sized magnesium oxide (M7) sample (prepared from glycine). For a typical experiment, 100 mg of the nanooxide sample was added to 25 ml of 0.06 ml/l Malathion solution which was kept in dark for 6 hrs. The degradation process was investigated as previously mentioned for Orange G dye and the concentration of the remaining pollutant was followed up by measuring absorption spectra at 238, 265 nm (λ_{\max} for Malathion) at different time intervals.

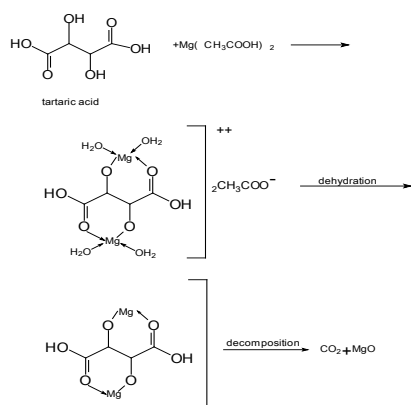
Antitumor activity

Antitumor activity against Breast Carcinoma MCF-7 cell line was measured for some selected samples at The Regional Center for Mycology and Biotechnology, Al-Azhar University, Cairo, Egypt and compared to that of Vinblastine as a standard drug. The number of viable cells and the percentage of viability were calculated as $(1 - \frac{OD_t}{OD_c}) \times 100$; where OD_t is the mean optical density of the wells treated with the tested samples and OD_c is the mean optical density of the untreated cells. The relation between surviving cells and drug concentration is plotted to get the survival curve of each tumor cell line after treatment with the nanooxides. The 50% inhibitory concentration (IC_{50}), the concentration required to cause toxic effect in 50% of intact cells, was estimated from graphic plots of the dose response curve for each concentration.

Results and Discussion

Characterization

Thermogravimetric analysis: The thermogravimetric-differential thermal analysis was performed on the organic precursors to follow their thermal decomposition to the final oxide forms. Inspection of the thermograms (Figure 1) showed that the organic precursors were thermally degraded through three main steps. The first within the temperature range 66.75-184.78°C due to the dehydration of humidity and crystallinity water (this step is sometimes a composite of two steps). The beginning of the thermal degradation of the anhydrous compounds took place within the second step within the temperature range 114.72-344.33°C by the evolution of gases such as N_2 and CO_2 . Complete decomposition of the organic precursors occurred in the third step within the range 232.99-565.99°C which led to the formation of the nanosized MgO as final product. Example of thermal decomposition process of tartaric acid precursor is represented as:



Fourier transforms infrared spectra (FTIR): The FTIR spectra of the magnesium-organic precursors were studied and compared to those of the corresponding nanooxides. The most important band frequencies (cm^{-1}) are listed in Table 1. The spectra of the organic precursors show weak absorption bands within the wavenumber ranges 3373-3430 cm^{-1} and 1033-1171 cm^{-1} due to the stretching and bending vibrations of the trace water molecule, respectively. These two bands appeared within the ranges 2955-3430 cm^{-1} and 1032-1176 cm^{-1} as very weak bands in the spectra of the ignited samples. The strong bands within the range 1570-1677 cm^{-1} are due to the stretching vibration of C=O group ($V_{C=O}$). These bands, more or less, disappeared in case of calcinated samples. It is worthy to mention that there is a shift in the IR active mode, which is due to nano size grain. For a nano size grain, the atomic arrangement on the boundaries differ greatly from that of the bulk crystals, both in coordination number and bond lengths, showing some extent of disorder [26]. Crystal symmetry is thus, degraded in nano size grains. The degradation in crystal symmetry results in the shifting of the IR active mode [27].

X-ray diffraction analysis (XRD): The X-ray diffraction patterns of the nano sized magnesium oxides are shown in Figure 2. The XRD sharp lines reveal that the oxide nanoparticles are crystalline. The relative crystalline sizes are determined from the XRD lines broadening using the Scherrer equation [28]. From calculation, the average crystalline size was found to be 44.8, 33.94, 44.60, 46.32, 47.16, 60.80 and 53.64 nm for magnesium oxides (M1-M7), respectively (Table 2). The phase purity of all the samples was established by comparison of the X-ray diffraction patterns with JCPDS international data value.

High resolution transmission electron microscopy (HRTEM): The micro structural analysis of the synthesized samples calcined at 650°C for 6 hours was investigated using HRTEM. The HRTEM images of some selected samples are shown in Figure 3. It can be seen from the graphs that magnesium nanoparticles have narrow size distribution and are rectangular rod shapes with weak agglomeration. The average particle sizes ranged from 33.93-60.80 nm.

Optical analysis: A fundamental property of nanosized metal oxides is the band gap energy. The band gap energy is the energy separation between the filled valence band and the empty conduction band. Optical excitation of electrons across the band gap is strongly allowed, producing an abrupt increase in the absorption at the wavelength corresponding to the band gap energy. The UV-Visible spectra allow direct determination of band gap using the relation

| Compound | IR frequency (cm^{-1}) | | | | |
|--------------|----------------------------|---------------|-----------|-------------|------|
| | ν_{OH} | δ_{OH} | $V_{C=O}$ | ν_{C-O} | Mg-O |
| Mg-oxalate | 3389 _{br} | 1128.96 | 1637 | 829.92 | 501 |
| NP (M1) | 2955 _{vw} | 1166.68 | --- | --- | 541 |
| Mg-tartrate | 3408 _{br} | 1090.45 | 1617 | 832.88 | 486 |
| NP (M2) | 2979 _{vw} | 1135.71 | --- | --- | 542 |
| Mg-citrate | 3425.52 | 115.64 | 1624 | 885 | 544 |
| NP (M3) | 3430 _{vw} | 1085 | --- | --- | 553 |
| Mg-succinate | 3430.71 | 1176.47 | 1691 | 893.54 | 522 |
| NP (M4) | 3110 _{vw} | 1152.45 | --- | --- | 544 |
| Mg-malate | 3404.33 _{br} | 1084.14 | 1570 | 870.23 | 579 |
| NP (M5) | 3052 _{vw} | 1171.25 | --- | --- | 570 |
| Mg-malonate | 3428 | 1032.77 | 1677 | 913.15 | 586 |
| NP (M6) | 3362 _{br} | 1136.70 | --- | --- | 583 |
| Mg-glycinate | 3373 _{br} | 1033.78 | 1617 | 924.83 | 512 |
| NP (M7) | 3381 | 1095.12 | --- | --- | 522 |

Table 1: IR frequencies (cm^{-1}) of some important groups in the organic precursors and the corresponding nanooxides.

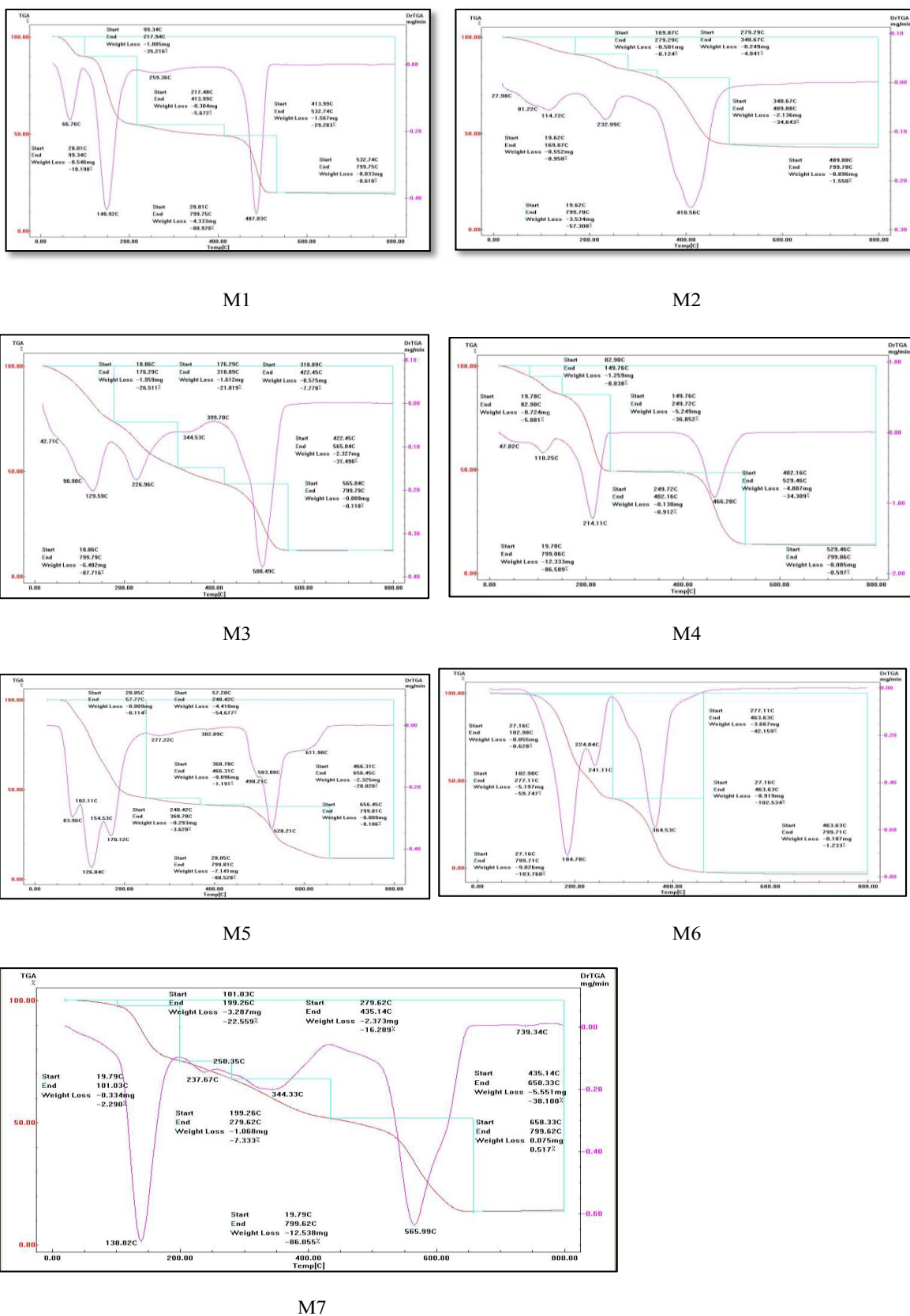


Figure 1: TGA-DTA curves for precursors M1- M7.

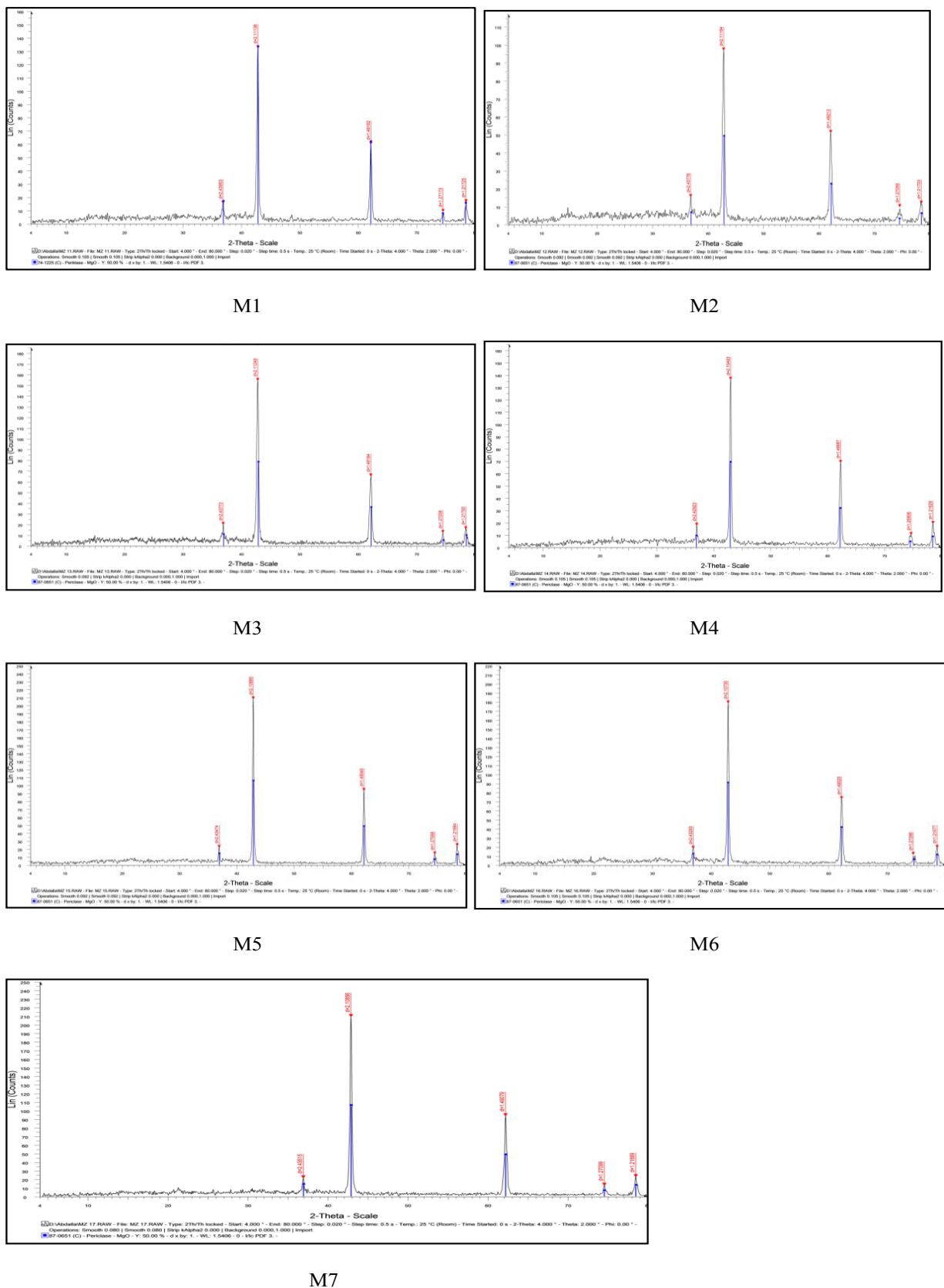


Figure 2: XRD of the samples M1- M7 prepared from organic precursors.

| Sample | Precursor | crystal size (nm) | Phase produced by XRD | Card No. | Crystal system |
|--------|-----------|-------------------|-----------------------|-------------|----------------|
| M1 | Oxalate | 44.80 | Periclase-MgO | 01-074-1225 | Cubic |
| M2 | Tartarate | 33.94 | Periclase-MgO | 01-087-0651 | Cubic |
| M3 | Citrate | 44.60 | Periclase-MgO | 01-087-0651 | Cubic |
| M4 | Succinate | 46.32 | Periclase-MgO | 01-087-0651 | Cubic |
| M5 | Malate | 47.16 | Periclase-MgO | 01-087-0651 | Cubic |
| M6 | Malonate | 60.80 | Periclase-MgO | 01-087-0651 | Cubic |
| M7 | Glycinate | 53.64 | Periclase-MgO | 01-087-0651 | Cubic |

Table 2: Effect of organic acids and glycine precursors on the crystal size and morphology of the prepared nanooxides.

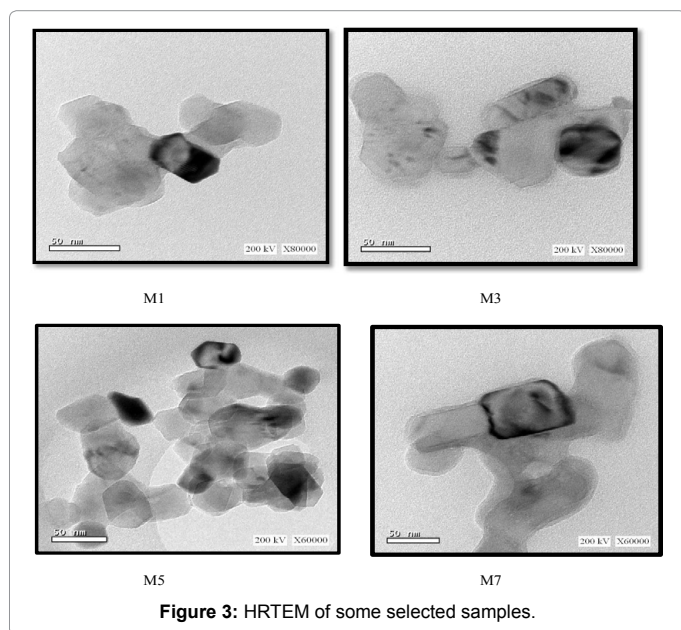


Figure 3: HRTEM of some selected samples.

between the absorption coefficient (α) and the incident photon energy ($h\nu$) represented by Tauc equation [29]:

$$(\alpha h\nu) = A(h\nu - E_g)^n$$

Where, A is a constant, E_g is the band gap of the material and exponent n depends on the type of transition, n is either 2 for an indirect transition or $\frac{1}{2}$ for a direct transition. Here the transition is direct so, n is taken to be $\frac{1}{2}$. The value of optical band gap is calculated by plotting the relation between $(\alpha h\nu)^2$ vs. $h\nu$ and extrapolating the straight line portion to the $h\nu$ axis. The extrapolation of linear portion to the $h\nu$ axis gives values of energy gap for magnesium oxide nanoparticles. The obtained E_g values (within the range 2.91-3.12 eV) show the semiconductor nature of the samples and are in an excellent agreement with the reported data [30].

Application

Photocatalytic degradation of organic G dye: The photodegradation efficiency of selected zirconium oxide nanoparticle (sample M3; prepared from citric acid as organic precursor) was tested using Orange G (OG) as model. The experiments were done at different conditions, namely; (UV+H₂O₂+M3), (UV+H₂O₂), (UV only), (UV+M3) where best results were obtained in the case of (UV+H₂O₂+M3). At periodic intervals of time, aliquots of the sample were withdrawn and the absorption spectra were recorded. Clearly, the absorbance decreases and the photodegradation efficiency increases (reaching a plateau) as a function of time (Figure 4). The results showed that the maximum percent of degradation of OG dye was 93% after 210 min indicating the very high efficiency of the nanoparticle used.

| Oxide | IC ₅₀ (µg/ml) |
|-------------|--------------------------|
| Vinblastine | 4.6 |
| M2 | 213 |
| M3 | 398 |
| M7 | 391 |

Table 3: Lethal concentration (IC50) of the nanosized oxides M2, Z3 and M27.

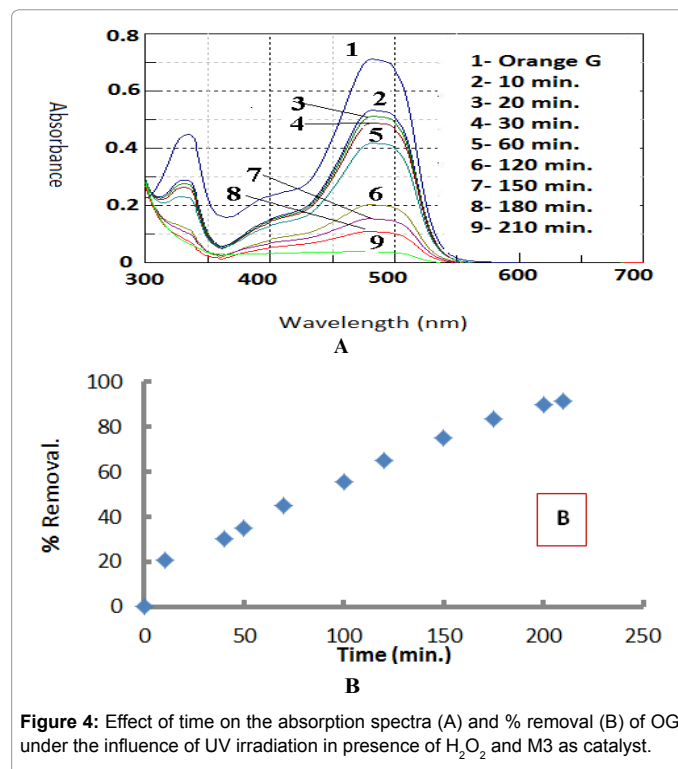


Figure 4: Effect of time on the absorption spectra (A) and % removal (B) of OG under the influence of UV irradiation in presence of H₂O₂ and M3 as catalyst.

Decomposition of chemical warfare agents on metal oxides: Metal oxides demonstrate superior ability to adsorb and decompose CWA compared to pure metal surfaces. This is often attributed to reactive sites on the metal oxide surface through which organophosphonate species (nerve agents) can adsorb and subsequently undergo a hydrolysis reaction. The use of MgO nanoparticle, M7, (prepared from glycine as precursor) as catalyst for the decontamination of VX stimulant Malathion was carefully investigated. The effect of different factors affecting the removal efficiency, such as: time, pH, temperature and initial dose of Malathion was studied. The results obtained (Figures 5 and 6) showed that such nanooxides have high ability for the removal of this pollutant from water samples.

Antitumor activity

Inhibitory activity against Breast Carcinoma MCF-7 cell line was detected using some selected nanosized metal oxides viz; M2

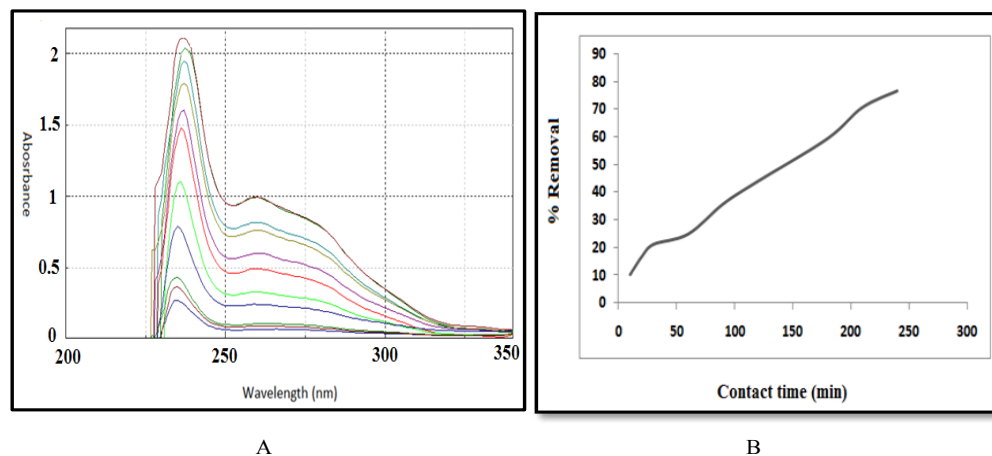


Figure 5: Effect of contact time on the absorption spectra of Malathion (A) and its % removal (B).

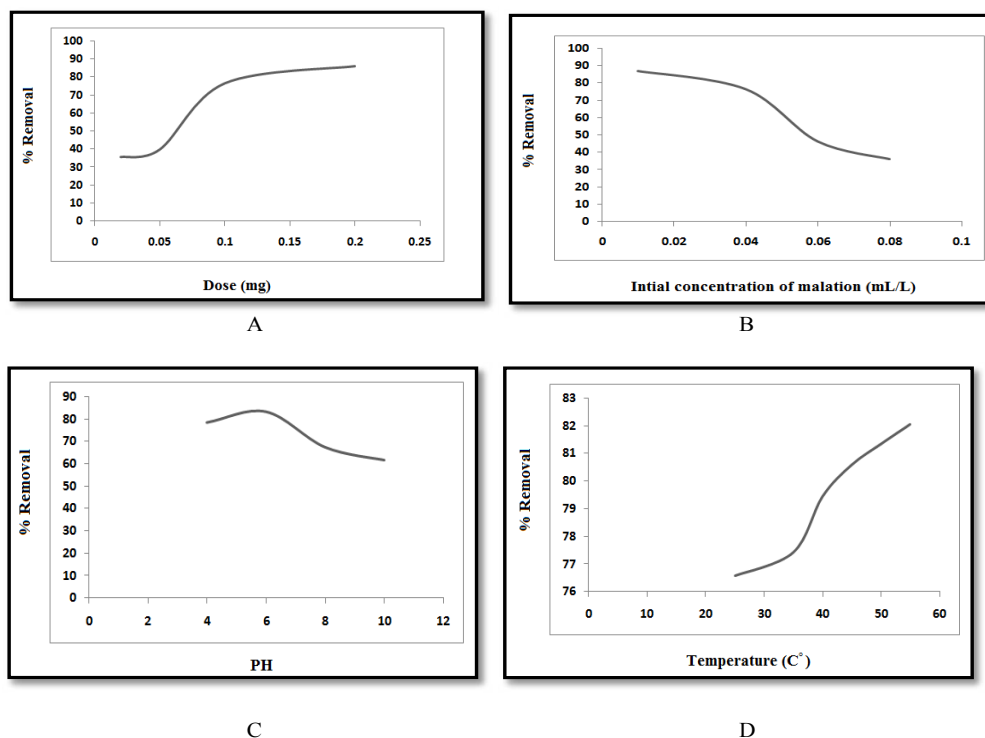


Figure 6: Effect of different factors on the % removal of Malathion; (A); adsorbent dose, (B); initial concentration, (C); pH and (D); temperature.

and M3 and M7 and compared to that of Vinblastine as a standard drug. The relation between surviving cells and drug concentration is plotted to get the survival curve of each tumor cell line after treatment with the nanooxides. The 50% inhibitory concentration (IC_{50}), the concentration required to cause toxic effect in 50% of intact cells, was estimated from graphic plots of the dose response curve for each concentration. The results are represented graphically in Figure 7 and the lethal concentrations (IC_{50}) values are listed in Table 3.

Inspection of the cytotoxic data, it is found that magnesium oxide M2 (prepared from tartaric acid) is, in general, more effective than those of M3 (prepared from citric acid) and M7 (prepared from

glycine). Shier [31] suggested that compounds having IC_{50} values 10-25 $\mu\text{g/ml}$ are considered to have weak cytotoxic activities, while those having intermediate values (ranging from 5-10 $\mu\text{g/ml}$) are classified as moderately active. On the other hand, compounds with IC_{50} values less than 5 $\mu\text{g/ml}$ are considered to be very active. Consequently, the nanosized metal oxides under study are considered to have weak activity with IC_{50} values higher than 213 $\mu\text{g/ml}$.

Conclusion

MgO nanoparticles (M1-M7) were prepared by precipitation of Mg as oxalate, tartarate, succinate, malate, malonate and glycinate then ignition at 650°C. The magnesium-organic precursors and the

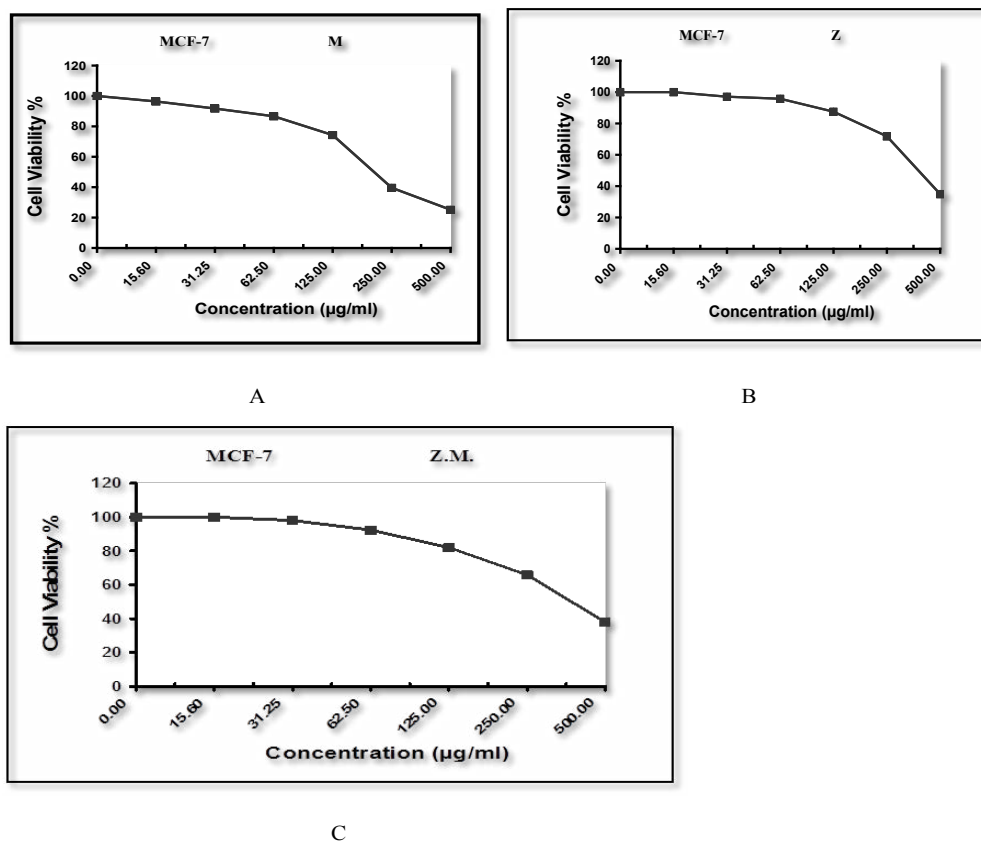


Figure 7: Inhibitory activity of nanooxideM2 (A), (IC₅₀=213 µg/ml), M3 (B), (IC₅₀=398 µg/ml) and M7 (C), (IC₅₀=391 µg/ml) against Breast carcinoma cells MCF-7.

corresponding nanooxides were characterized by thermal analysis and different spectroscopic techniques. The morphology and crystal sizes were found to be highly affected by the starting organic precursors. The optical energy gaps (E_g) calculated from electronic absorption spectra ranged from 2.91 to 3.12 eV suggesting the semiconductor nature of the nanooxides. The results revealed that the prepared inexpensive magnesium oxides have high potential as catalysts for photo degradation of both Malathion and orange G from water samples. Inhibitory activity against Breast Carcinoma MCF-7 cell line was detected using some selected nanosized MgO and compared to that of Vinblastine as a standard drug.

Acknowledgement

We would like to acknowledge the financial support from the MSP (Management of Scientific Projects), Benha University, Benha, Egypt (project presented by I. M. Ibrahim).

References

- Neppolian B, Wang Q, Yamashita H, Choi H (2007) Synthesis and characterization of ZrO₂-TiO₂ binary oxide semiconductor nanoparticles: application and interparticle electron transfer process. *Applied Catalysis A: General* 333: 264-271.
- Lara-García HA, Romero-Ibarra IC, Pfeiffer H (2014) Hierarchical Na-doped cubic ZrO₂ synthesis by a simple hydrothermal route and its application in biodiesel production. *Journal of Solid State Chemistry* 218: 213-220.
- Słońska A, Kaszewski J, Wolska-Kornio E, Witkowski B, Mijowska E, et al. (2016) Luminescent properties of ZrO₂: Tb nanoparticles for applications in neuroscience. *Optical Materials* 59: 96-102.
- Xiong C, Wang W, Tan F, Luo F, Chen J, et al. (2015) Investigation on the efficiency and mechanism of Cd(II) and Pb(II) removal from aqueous solutions using MgO nanoparticles. *Journal of hazardous materials* 299: 664-674.
- Li S, Jiao Y, Wang Z, Wang J, Zhu Q, et al. (2015) Performance of RP-3 kerosene cracking over Pt/WO₃-ZrO₂ catalyst. *Journal of Analytical and Applied Pyrolysis* 113: 736-742.
- Renuka L, Anantharaju KS, Sharma SC, Nagaswarupa HP, Prashantha SC, et al. (2016) Hollow microspheres Mg-doped ZrO₂ nanoparticles: Green assisted synthesis and applications in photocatalysis and photoluminescence. *Journal of Alloys and Compounds* 672: 609-622.
- Peng W, Li J, Chen B, Wang N, Luo G, et al. (2016) Mesoporous MgO synthesized by a homogeneous-hydrothermal method and its catalytic performance on gas-phase acetone condensation at low temperatures. *Catalysis Communications* 74: 39-42.
- Varshney D, Dwivedi S (2015) On the synthesis, structural, optical and magnetic properties of nano-size Zn-MgO. *Superlattices and Microstructures* 85: 886-893.
- Gh AB, Sabbaghan M, Mirgani Z (2015) A comparative study on properties of synthesized MgO with different templates. *Spectrochimica Acta Part A: Molecular and Biomolecular Spectroscopy* 137: 1286-1291.
- Klubnuan S, Amornpitoksuk P, Suwanboon S (2015) Structural, optical and photocatalytic properties of MgO/ZnO nanocomposites prepared by a hydrothermal method. *Materials Science in Semiconductor Processing* 39: 515-520.
- Li H, Li M, Qiu G, Li C, Qu C, et al. (2015) Synthesis and characterization of MgO nanocrystals for biosensing applications. *Journal of Alloys and Compounds* 632: 639-644.
- Jin Z, Jia Y, Luo T, Kong LT, Sun B, et al. (2015) Efficient removal of fluoride by hierarchical MgO microspheres: performance and mechanism study. *Applied Surface Science* 357: 1080-1088.
- Ding YD, Song G, Zhu X, Chen R, Liao Q (2015) Synthesizing MgO with a high specific surface for carbon dioxide adsorption. *RSC Advances* 5: 30929-30935.

14. Verma R, Naik KK, Gangwar J, Srivastava AK (2014) Morphology, mechanism and optical properties of nanometer-sized MgO synthesized via facile wet chemical method. *Materials Chemistry and Physics* 148: 1064-1070.
15. Yadav LR, Lingaraju K, Manjunath K, Raghu GK, Kumar KS, et al. (2017) Synergistic effect of MgO nanoparticles for electrochemical sensing, photocatalytic-dye degradation and antibacterial activity. *Materials Research Express* 4: 025028.
16. Devaraja PB, Avadhani DN, Prashantha SC, Nagabhushana H, Sharma SC, et al. (2014) Synthesis, structural and luminescence studies of magnesium oxide nanopowder. *Spectrochimica Acta Part A: Molecular and Biomolecular Spectroscopy* 118: 847-851.
17. Moussavi G, Mahmoudi M (2009) Removal of azo and anthraquinone reactive dyes from industrial wastewaters using MgO nanoparticles. *Journal of Hazardous Materials* 168(2): 806-812.
18. Moussavi G, Mahmoudi M (2009) Degradation and biodegradability improvement of the reactive red 198 azo dye using catalytic ozonation with MgO nanocrystals. *Chemical Engineering Journal* 152: 1-7.
19. Bindhu MR, Umadevi M, Micheal MK, Arasu MV, Al-Dhabi NA (2016) Structural, morphological and optical properties of MgO nanoparticles for antibacterial applications. *Materials Letters* 166: 19-22.
20. Hamdy MS, Awwad NS, Alshahrani AM (2016) Mesoporous magnesia: Synthesis, characterization, adsorption behavior and cytotoxic activity. *Materials & Design* 110: 503-509.
21. Rao PV, Nallappan D, Madhavi K, Rahman S, Jun Wei L, et al. (2016) Phytochemicals and biogenic metallic nanoparticles as anticancer agents. *Oxidative medicine and cellular longevity*.
22. Krishnamoorthy K, Manivannan G, Kim SJ, Jeyasubramanian K, Premanathan M (2012) Antibacterial activity of MgO nanoparticles based on lipid peroxidation by oxygen vacancy. *Journal of Nanoparticle Research* 14: 1063.
23. Tang ZX, Lv BF (2014) MgO nanoparticles as antibacterial agent: preparation and activity. *Brazilian Journal of Chemical Engineering* 31: 591-601.
24. Yadav LR, Lingaraju K, Manjunath K, Raghu GK, Kumar KS, et al. (2017) Synergistic effect of MgO nanoparticles for electrochemical sensing, photocatalytic-dye degradation and antibacterial activity. *Materials Research Express* 4: 025028.
25. Ibrahim IM, Moustafa ME, Abdelhamid MR (2016) Effect of organic acids precursors on the morphology and size of ZrO₂ nanoparticles for photocatalytic degradation of Orange G dye from aqueous solutions. *Journal of Molecular Liquids* 223: 741-748.
26. Yua J, Kimb D (2013) *Powder Tech* 235: 1030-1037.
27. Motlagh MK, Youzbashi AA, Sabaghzadeh L (2011) Synthesis and characterization of Nickel hydroxide/oxide nanoparticles by the complexation-precipitation method. *International Journal of Physical Sciences* 6: 1471-1476.
28. Arora K, Devi S (2012) current trends in biotech and chem. *Research* 2.
29. Chang-Sam K, Dond-Hun Y, Sung-Woon J, Hyok-Bo K, Sang-Hwan P (2010) *J Korean Cryst, Growth Cryst Tech* 20: 283-288.
30. Dhare SL (2015) Silica-zirconia alkali-resistant coatings by sol-gel route. *Curr Sci* 108: 1647-1652.
31. Shier WT (1991) *Mammalian cell culture on \$5 a day: a laboratory manual of low cost methods*. Los Banos, University of the Philippines 64: 9-16.